Nano Res. 2012, 5(1): 43–48
DOI 10.1007/s12274-011-0183-0
Research Article

ISSN 1998-0124
CN 11-5974/O4

Strain-Induced Semiconductor to Metal Transition in the Two-Dimensional Honeycomb Structure of MoS_2

Emilio Scalise[1] (✉), Michel Houssa[1], Geoffrey Pourtois[2,†], Valery Afanas'ev[1], and André Stesmans[1]

[1] Semiconductor Physics Laboratory, Department of Physics and Astronomy, University of Leuven, Leuven B-3001, Belgium
[2] Department of Chemistry, University of Antwerp, Wilrijk-Antwerp B-2610, Belgium
[†] Present address: Interuniversity Microelectronics Centre, Leuven B-3001, Belgium

Received: 13 September 2011 / Revised: 25 October 2011 / Accepted: 25 October 2011

ABSTRACT

The electronic properties of two-dimensional honeycomb structures of molybdenum disulfide (MoS_2) subjected to biaxial strain have been investigated using first-principles calculations based on density functional theory. On applying compressive or tensile bi-axial strain on bi-layer and mono-layer MoS_2, the electronic properties are predicted to change from semiconducting to metallic. These changes present very interesting possibilities for engineering the electronic properties of two-dimensional structures of MoS_2.

KEYWORDS

MoS_2, quasi-2D chalcogenide materials, first-principles modeling, strain-induced semiconductor to metal transition

1. Introduction

Molybdenum disulfide (MoS_2) is an indirect band gap semiconductor, consisting of S–Mo–S sheets with a hexagonal structure like graphene, silicene or germanene [1–6]. Recently, the structural similarity between these materials and the possibility to create ultra-thin films (down to a mono-layer) of MoS_2, exploiting its quantum effects, have attracted a lot of interest [7–15]. The formation of suspended mono-layer MoS_2 has been recently demonstrated [7, 8] and its properties have been investigated both experimentally [9–11] and theoretically [10–14]. Furthermore, mono-layer MoS_2 has been recently used as a conductive channel to realize a low-power field-effect transistor [15]. Single layer MoS_2 is a direct-gap semiconductor with a band gap of about 1.9 eV [9–11], so potentially interesting for electronic, optoelectronic and photo-voltaic applications.

In this work, we investigate the evolution of the electronic properties of bulk and layered MoS_2, going from a few layers down to a mono-layer and then study the effect of bi-axial strain on the electronic structure. We observe a progressive shrinking of the energy band gap upon increasing the applied strain. Both for tensile and compressive strain, a transition limit is reached where the bottom of the conduction band and the top of the valence band cross the Fermi energy, changing the nature of the system from semiconducting to metallic. The application of strain on the two-dimensional (2D) structures of MoS_2 could thus potentially be used to tune its electronic transport properties, from semiconducting to semimetallic, and ultimately to metallic.

Address correspondence to Emilio.Scalise@fys.kuleuven.be

2. Experimental

2.1 Calculation methods

The first-principles calculations were performed within the density-functional theory (DFT) using the generalized gradient approximation (GGA) proposed by Perdew, Burke, and Ernzerhof [16] for the exchange and correlation energy, as implemented in the Quantum ESPRESSO package [17] with the addition of a semi-empirical dispersion term [18, 19]. The valence electrons for sulfur and the valence and semi-core states (4s and 4p) for molybdenum were explicitly treated in the calculations using ultrasoft pseudopotentials [20]. The electronic wavefunctions were described by plane-wave basis sets with a kinetic energy cutoff of 28 Ry, and the energy cutoff for the charge density was set to 280 Ry. For the band structure calculations, 300 *K*-points were chosen, along the lines connecting the high-symmetric points in reciprocal space. A threshold of 10^{-4} Ry/Bohr on the force for the ionic relaxation and of 0.05 GPa on the pressure for the cell relaxation were used.

2.2 Mono-layer and bi-layer MoS_2 models

The hexagonal structure of molybdenum disulfide with the lattice parameters $a = b = 3.16$ Å and $c = 12.29$ Å [21–23] was taken as starting point for the geometry relaxation. The calculated energy band gap for the optimized structure of bulk MoS_2 is 1.18 eV, in excellent agreement with the experimental value (1.23 eV [21]). In fact, the addition of the semi-empirical term accounting for dispersion provides a better estimation of the energy band gap with respect to previous GGA calculations [14, 24]. This is mainly due to a better estimation of the interlayer interaction and, consequentially, a better value of the *c*-axis crystal parameter, which is calculated to be 13.07 Å; previous GGA calculations, not including the dispersion term, typically overestimated the *c*-axis parameter by about 2 Å [14]. We then built structures of multilayer MoS_2 sheets, starting with the lattice parameters of the bulk relaxed MoS_2. The S–Mo–S sheets were placed in large supercells with about 10 Å of vacuum between the periodic replica. After geometry relaxation, the multilayer MoS_2 structures with 1, 2 and 4 S–Mo–S sheets did not show significant differences in term of Mo–S bond lengths and S–S distances with respect to the bulk structure, while their energy band gaps increased with decreasing number of layers (Fig. 1(a)). In particular, one observes a progressive change in the indirect energy gap from the bulk value to about 2 eV for mono-layer MoS_2. In contrast, the change in the direct-gap is not significant, with a shift of only 0.1 eV from the bulk to the mono-layer. As a result, the indirect–direct-gap crossover is reached in the limit of the mono-layer MoS_2 (see Fig. 1(b)), with the bi-layer having a very small energy difference between direct and indirect energy gap (see also Fig. 1(c)).

Note that the computed energy band gaps (B. G.) for the mono- (direct B. G. = 1.72 eV, indirect B. G. = 1.98 eV) and bi-layer MoS_2 (direct B. G. = 1.7 eV, indirect B. G. = 1.52 eV) are in good agreement with experimental results [9–11].

2.3 Application of biaxial strain

We then apply a biaxial strain on mono-layer and bi-layer MoS_2 by changing the in-plane (*a* and *b*, equally) cell parameters, relaxing the structure along the *c*-axis (the direction perpendicular to the S–Mo–S sheets), since on applying an in-plane biaxial strain a deformation in the perpendicular (*z*) direction is likely. As expected, not only the Mo–S bond length d_{Mo-S}, but also the distance between the S atoms (within a S–Mo–S sheet) d_{S-S} varies with the applied strain (see Tables 1 and 2). This has a significant impact on the band structure of strained 2D-MoS_2, as discussed below.

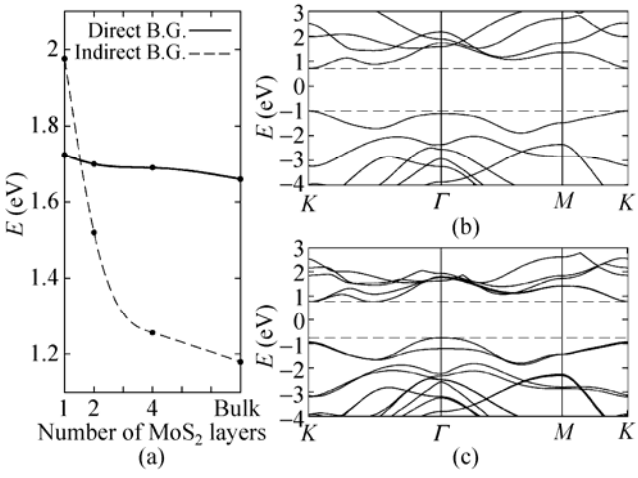

Figure 1 (a) Plot of the energy band gap (E_g) versus number of S–Mo–S sheets in multilayer MoS_2, the Fermi level is set at 0 eV. Energy band structures of mono-layer (b) and bi-layer (c) MoS_2

Table 1 Calculated structural parameters (Mo–S bond lengths, d_{Mo-S}; S–S bond lengths, d_{S-S}; S–Mo–S bond angle, θ(S–Mo–S)) and energy band gap for mono-layer MoS_2 as a function of the applied strain; negative values of the band gap indicate overlapping of conduction and valence bands

Tensile strain (%)	d_{Mo-S} (Å)	d_{S-S} (Å)	θ(S–Mo–S)	E_g (eV)	Compr. strain (%)	d_{Mo-S} (Å)	d_{S-S} (Å)	θ(S–Mo–S)	E_g (eV)
0.00	2.43	3.15	80.68	1.72 (dir.)	0.00	2.43	3.15	80.68	1.7272 (dir.)
2.00	2.44	3.10	78.80	1.35 (ind.)	2.00	2.42	3.19	82.54	1.74 (ind.)
5.00	2.47	3.05	76.20	0.77 (ind.)	5.00	2.40	3.26	85.44	1.52 (ind.)
8.00	2.50	3.00	73.69	0.29 (ind.)	8.00	2.39	3.33	88.45	1.27 (ind.)
10.00	2.51	2.94	71.69	–0.03 (ind.)	10.00	2.38	3.38	90.47	1.09 (ind.)
13.00	2.52	2.84	68.51	–0.42 (ind.)	13.00	2.37	3.46	93.67	0.53 (ind.)
15.00	2.54	2.80	66.85	–0.56 (ind.)	15.00	2.38	3.55	96.65	–0.25 (ind.)

Table 2 Calculated structural parameters (Mo–S bond lengths, d_{Mo-S}; S–S bond lengths, d_{S-S}; S–Mo–S bond angle, θ(S–Mo–S)) and energy band gap for bi-layer MoS_2 as a function of the applied strain; negative values of the band gap indicate overlapping of conduction and valence bands

Tensile strain (%)	d_{Mo-S} (Å)	d_{S-S} (Å)	θ(S–Mo–S)	E_g (eV)	Compr. strain (%)	d_{Mo-S} (Å)	d_{S-S} (Å)	θ(S–Mo–S)	E_g (eV)
0.00	2.43	3.15	80.73	1.52 (dir.)	0.00	2.43	3.15	80.73	1.52 (dir.)
2.00	2.44	3.10	78.90	1.05 (ind.)	2.00	2.42	3.19	82.60	1.55 (ind.)
5.00	2.47	3.05	76.26	0.48 (ind.)	5.00	2.40	3.26	85.50	1.30 (ind.)
8.00	2.49	2.98	73.69	0.00 (ind.)	8.00	2.39	3.33	88.50	1.09 (ind.)
10.00	2.50	2.92	71.69	–0.29 (ind.)	10.00	2.38	3.38	90.55	0.90 (ind.)
13.00	2.52	2.84	68.51	–0.59 (ind.)	13.00	2.37	3.46	93.73	0.40 (ind.)
15.00	2.54	2.80	66.85	–0.72 (ind.)	15.00	2.38	3.55	96.67	–0.40 (ind.)

3. Results and discussion

A first general observation for the band structures of strained 2D-MoS_2 is the reduction of the energy band gap with increasing applied strain (both tensile and compressive), as illustrated in Fig. 2, confirming previous calculations on the variation of the energy band gap as a function of pressure in bulk MoS_2 [24].

To gain insight into the changes in the electronic properties of the 2D-MoS_2 structures as a function of the applied strain, we investigated in detail the variation of the band structures and discuss the most significant results, presented in Figs. 3 and 4 for mono- and bi-layer MoS_2, respectively. All the significant changes in the band structure of the quasi-2D MoS_2 occurring on application of bi-axial strain can be related to shifts in the energy states of the valence band near the Γ point and of the conduction band between the K and the Γ points, and to a lesser extent, of the conduction and valence band near the K point. Analysis of the partial density of states (not shown) indicates that these states mainly originate from the 3p orbitals of S atoms and 4d orbitals of Mo atoms. When the distances between the atoms change (due to the applied strain), a different superposition of their atomic orbitals leads to a shift of the energy of these states. A similar trend was observed for the variation of the energy band structure of layered MoS_2 on changing the distance between the S–Mo–S sheets and their number [13]. In this case, however, only changes in the overlap between the $3p_z$ orbitals of S and $4d_{z^2}$ orbitals of Mo (i.e., along the direction perpendicular to the S–Mo–S sheets) were involved, resulting in a shift at the top of the valence band near the Γ point and a shift (in the opposite direction) of the bottom of the conduction band between the K and the Γ points, as is also evident in Figs. 1(b) and 1(c) for mono-layer and bi-layer MoS_2, respectively. Upon the application of bi-axial strain, the distances between the Mo and S atoms are changed along the S–Mo–S sheets (xy plane) as well as in the

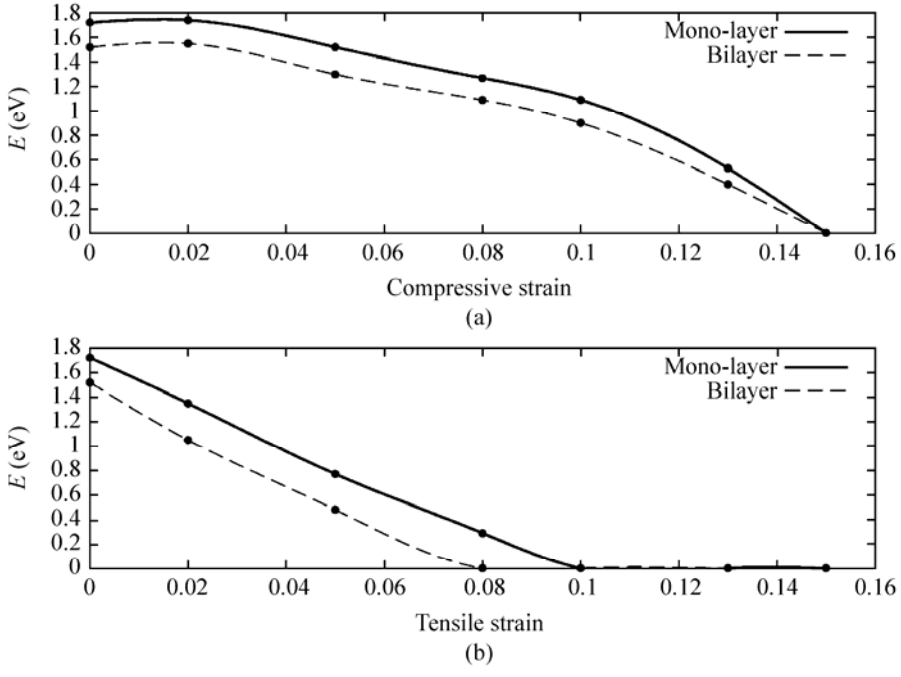

Figure 2 Plots of energy band gap (E_g) versus applied strain for mono- and bi-layer MoS_2

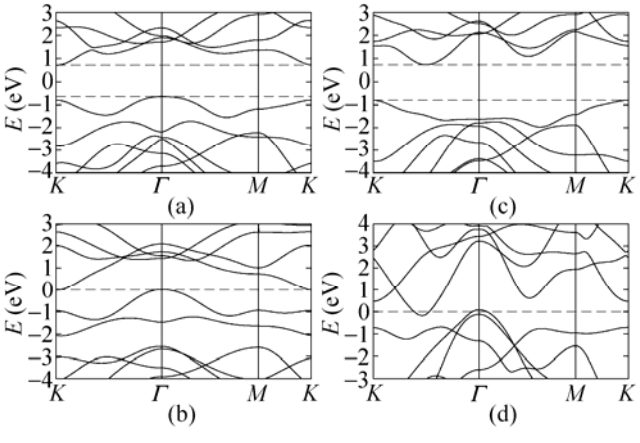

Figure 3 Energy band structures of mono-layer MoS_2 with different applied strain: 2% (a) and 10% (b) tensile; 5% (c) and 15% (d) compressive. The Fermi level is set at 0 eV

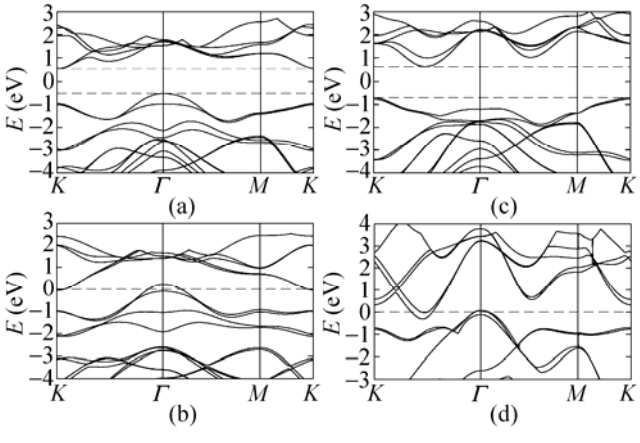

Figure 4 Energy band structures of bi-layer MoS_2 with different applied strain: 2% (a) and 10% (b) tensile; 5% (c) and 15% (d) compressive. The Fermi level is set at 0 eV

perpendicular direction (see Tables 1 and 2). The variations in the energy band structures are then more complex and involve not only the top of the valence band near the Γ point and the bottom of the conduction band between the K and Γ points, but also the bands at the K point and inner states at the Γ point (primarily composed of orbitals localized in the xy plane). More particularly, tensile strain causes a rise of the energy at the top of the valence band near the Γ point and at the bottom of the conduction band between the K and the Γ points, as shown in Figs. 3(a) and 3(b), likely induced by the reduction of the distance between the S atoms (d_{S-S}) and the increase of the distance between the Mo and S atoms (d_{Mo-S}); note that the top of the valence band and the bottom of the conduction band near the K point undergo much less significant changes. Such a shift of the energy levels results into a change in the nature of the energy band gap for the mono-layer MoS_2, from direct to indirect, even for an applied tensile strain of less then 2%, see Fig. 3(a). A progressive reduction of the energy band gap with respect to the applied strain is then observed up to about 10%

(Fig. 3(b)), when the system becomes semi-metallic. For such a tensile strain, the bottom of the conduction band at the *K* point and the top of the valence band at the *Γ* point cross the Fermi level. For larger strain, the system then moves towards a metallic behavior. Note also that from the analysis of the stress–strain curve (not shown here), we calculated a Young's modulus of about 435 GPa for the mono-layer. The point of ultimate tensile strength is estimated at about 43 GPa, corresponding to a tensile strain of 20%, with the linear elastic region extending to a stress of about 9.5%. Therefore, we have indications that the semiconductor–metal transition limit could be reached in realistic situations.

The changes in the band structure of bi-layer MoS_2 with the applied tensile strain are very similar to those of the mono-layer, as illustrated in Figs. 4(a) and 4(b). The main difference arises from the value of the energy band gap, which is lower for the bi-layer system, due to the energy contribution of the interlayer interaction. The semiconductor–metal crossover of the tensile strained bi-layer is thus reached at a lower value of the strain (about 8%).

An opposite trend for the shifts of the energy bands is observed in the case of compressive bi-axial strain. In this case, both the top of the valence band near the *Γ* point and the bottom of the conduction band between the *K* and *Γ* points drop substantially with increasing applied strain. In contrast, the valence and conduction bands at the *K* point rises. For a relatively small strain (below 5%), compressive and tensile strain show opposite effects on the band structure: the band gap is reduced when tensile strain is applied to both mono- and bi-layer MoS_2, but it is (slightly) increased under compressive strain (see Tables 1 and 2). Note that both compressive and tensile strain cause a direct to indirect band gap transition even for small applied strain. This is due to the fact that the energy difference between the relative maximum (minimum) of the valence (conduction) band located at different *K*-points is very small and a slight change in the distance between the atoms is sufficient to shift the energy states, breaking the direct band gap symmetry.

For applied strain below typically 5%, only the energy states at the edge of the band gap (primarily composed of p_z orbitals and d_{z^2} orbitals) are involved. When larger compressive strain is applied, the overlapping of the in-plane *xy* atomic orbitals is much more significant and consequently the shift of the energy is considerable also for the inner energy states. Particularly the energy bands at around –2 eV (mainly composed of in-plane d_{xy} and $d_{x^2-y^2}$ orbitals [23]) rise, overcoming the energy states of the d_{z^2} and p_z orbitals, (the edges of the band gap for small applied strain). With a 15% biaxial compressive strain applied to mono-layer and bi-layer MoS_2, this shift of the inner bands is so large that the top of the valence band and the bottom of the conduction band cross the Fermi level, as illustrated in Figs. 3(d) and 4(d). In the case of compressive strain, the semiconductor to metal transition is thus also observed, but involves a slightly different physical mechanism than that for tensile strain.

No significant differences between the band structures of the mono-layer and bi-layer MoS_2 are observed for both tensile and compressive bi-axial strain, indicating that the orbital interactions between atoms in the same S–Mo–S sheets are significantly more important than the interlayer interactions. Interestingly, significant changes in the curvature of the conduction and valence bands near their extrema (see Figs. 3 and 4) are predicted upon the application of strain (but are not expressly investigated here), suggesting the opportunity to use strain to modify the effective masses of the carriers in the 2D-MoS_2 structures. Finally, note that in our simulations, strain was applied with the same magnitude in the *x* and *y* directions, i.e. uniaxial or asymmetric strain in the *x*–*y* directions were not investigated. From our simulations, we can infer that applying an asymmetric strain in the (*x*–*y*) directions of mono- and bi-layer MoS_2 could tune their energy gap, also preserving their direct-gap behavior.

4. Conclusion

The electronic properties of quasi-2D MoS_2 have been investigated, focusing on the consequences of bi-axial strain. Mono-layer MoS_2 is predicted to be a direct-gap semiconductor (E_g = 1.72 eV), while bi-layer MoS_2 is found to be an indirect gap compound (E_g = 1.52 eV). The energy band gap of the mono- and bi-layer systems decreases upon the application of bi-axial

strain. Very interestingly, a semiconductor–metal transition is predicted for a tensile strain of about 8% or a compressive strain of about 15%. For mono-layer MoS_2 a transition from direct-to-indirect gap is also observed upon the application of relatively small strain (~2%). Our results thus indicate a very promising way of engineering the electronic properties of quasi-2D MoS_2 structures.

Acknowledgements

Part of this work was financially supported by the Fonds Wetenschappelijk Onderzoek (FWO) (project G.0628.09) and the Research Funds of K. U. Leuven (project OT/09/031).

References

[1] Geim, A. K; Novoselov, K. S. The rise of graphene. *Nat. Mater.* **2007**, *6*, 183–191.

[2] Fuhrer, M. S.; Lau, C. N.; MacDonald, A. H. Graphene: Materially better carbon. *MRS Bull.* **2010**, *35*, 289–295.

[3] Lebègue, S.; Eriksson, O. Electronic structure of two-dimensional crystals from *ab initio* theory. *Phys. Rev. B* **2009**, *79*, 115409.

[4] Cahangirov, S.; Topsakal, M.; Akturk, E.; Sahin, H.; Ciraci, S. Two- and one-dimensional honeycomb structures of silicon and germanium. *Phys. Rev. Lett.* **2009**, *102*, 236804.

[5] Houssa, M.; Pourtois, G.; Afanas'ev, V. V.; Stesmans, A. Electronic properties of two-dimensional hexagonal germanium. *Appl. Phys. Lett.* **2010**, *96*, 082111.

[6] Houssa, M.; Pourtois, G.; Afanas'ev, V. V.; Stesmans, A. Can silicon behave like graphene? A first-principles study. *Appl. Phys. Lett.* **2010**, *97*, 112106.

[7] Coleman, J. N.; Lotya, M.; O'Neill, A.; Bergin, S. D.; King, P. J.; Khan, U.; Young, K.; Gaucher, A.; De, S.; Smith, R. J., et al. Two-dimensional nanosheets produced by liquid exfoliation of layered materials. *Science* **2011**, *331*, 568–571.

[8] Novoselov, K. S.; Jiang, D.; Schedin, F.; Booth, T. J.; Khotkevich, V. V.; Morozov, S. V.; Geim, A. K. Two-dimensional atomic crystals. *Proc. Natl. Acad. Sci. USA* **2005**, *102*, 10451–10453.

[9] Mak, K. F.; Lee, C.; Hone, J.; Shan, J.; Heinz, T. F. Atomically thin MoS_2: A new direct-gap semiconductor. *Phys. Rev. Lett.* **2010**, *105*, 136805.

[10] Splendiani, A.; Sun, L.; Zhang, Y.; Li, T.; Kim, J.; Chim, C. Y.; Galli, G.; Wang, F. Emerging photoluminescence in monolayer MoS_2. *Nano Lett.* **2010**, *10*, 1271–1275.

[11] Han, S. W.; Kwon, H.; Kim, S. K.; Ryu, S.; Yun, W. S.; Kim, D. H.; Hwang, J. H.; Kang, J. S.; Baik, J.; Shin, H. J., et al. Band-gap transition induced by interlayer van der waals interaction in MoS_2. *Phys. Rev. B* **2011**, *84*, 045409.

[12] Lebegue, S.; Eriksson, O. Electronic structure of two-dimensional crystals from *ab initio* theory. *Phys. Rev. B* **2009**, *79*, 115409.

[13] Li, T.; Galli, G. Electronic properties of MoS_2 nanoparticles. *J. Phys. Chem. C* **2007**, *111*, 16192–16196.

[14] Ataca, C.; Sahin, H.; Akturk, E.; Ciraci, S. A comparative study of lattice dynamics of three- and two-dimensional MoS_2. *J. Phys. Chem. C* **2011**, *115*, 3934–3941.

[15] Radisavljevic, B.; Radenovic, A.; Brivio, J.; Giacometti, V.; Kis, A. Single-layer MoS_2 transistors. *Nat. Nanotechnol.* **2011**, *6*, 147–150.

[16] Perdew, J. P.; Burke, K.; Ernzerhof, M. Generalized gradient approximation made simple. *Phys. Rev. Lett.* **1996**, *77*, 3865–3868.

[17] Giannozzi, P.; Baroni, S.; Bonini, N.; Calandra, M.; Car, R.; Cavazzoni, C.; Ceresoli, D.; Chiarotti, G. L.; Cococcioni, M.; Dabo, I., et al. Quantum espresso: A modular and open-source software project for quantum simulations of materials. *J. Phys.: Cond. Matt.* **2009**, *21*, 395502.

[18] Grimme, S. Semiempirical GGA-type density functional constructed with a long-range dispersion correction. *J. Comp. Chem.* **2006**, *27*, 1787–1799.

[19] Barone, V.; Casarin, M.; Forrer, D.; Pavone, M.; Sambi, M.; Vittadini, A. Role and effective treatment of dispersive forces in materials: Polyethylene and graphite crystals as test cases. *J. Comp. Chem.* **2009**, *30*, 934–939.

[20] Vanderbilt, D. Soft self-consistent pseudopotentials in a generalized eigenvalue formalism. *Phys. Rev. B* **1990**, *41*, 7892–7895.

[21] Kam, K. K.; Parkinson, B. Detailed photocurrent spectroscopy of the semiconducting group VIB transition metal dichalcogenides. *J. Chem. Phys.* **1982**, *86*, 463–467.

[22] Young, P. A. Lattice parameter measurements on molybdenum disulphide. *Brit. J. Appl. Phys. (J. Phys. D)* **1968**, *1*, 936–938.

[23] Boker, T.; Severin, R.; Muller, A.; Janovitz, C.; Manzke, R.; Voss, D.; Kruger, P.; Mazur, A.; Pollmann, J. Band structure of MoS_2, $MoSe_2$, and α-$MoTe_2$: Angle-resolved photoelectron spectroscopy and *ab initio* calculations. *Phys. Rev. B* **2001**, *64*, 235305.

[24] Li, W.; Chen, J. F.; He, Q.; Wang, T. Electronic and elastic properties of MoS_2. *Physica B* **2010**, *405*, 2498–2502.